Design of Surface Acoustic Wave Motors With Non-piezoelectric Stator Material

Richard Günther, René Richter and Jens Lienig
Institute of Electromechanical and Electronic Design
Dresden University of Technology
Dresden, Germany
Email: richard.guenther@tu-dresden.de, rene.richter@tu-dresden.de and jens@ieee.org

***Abstract*—Surface Acoustic Wave (SAW) motors are specific piezoelectric motors that use traveling waves instead of the stator's natural vibration. Despite their promising potential due to their high blocking forces, high positioning accuracy and simple design, practical applications of these novel motors are still missing. Hence, we present guidelines for designing such an SAW motor. By focusing on a non-piezoelectric stator material, a wide range of stator materials can potentially be used. First, we introduce the structure of a Finite Element Method (FEM) analysis, which allows for the application and design of piezoelectric units. Furthermore, a numerical motor model is described, which calculates characteristics of such a motor. The focus is on expansions, considering the dynamic losses of the motor, as well as roughness and flatness of its contact surfaces. Our findings allow the design and improvement of SAW motors with non-piezoelectric stator material, thus contributing to their first practical application.**

***Index Terms*—piezoelectric motor, ultrasonic motor, SAW motor, Rayleigh waves, PZT**

I. Introduction

The availability of increasingly favorable and more compact control technologies allows the use of actuators with complex controls and the numerous use of small drives in general. Thus, there is – aside from a more frequented use of electronic commutated electromagnetic motors – a wide range of novel piezoelectric motors presented in the literature [1]–[5]. A special type of piezoelectric motor is the Surface Acoustic Wave (SAW) motor, which uses traveling waves instead of the stator's natural vibration [6]. Due to the high operation frequency it yields a very high power density and allows for powerful miniaturized linear motors. The latter are used for mirror adjusters in industrial sector or autofocus functionality in consumer lenses. When the SAW travels over the stator's surface, each point of the surface oscillates elliptically. According to Fig. 1, this behavior allows for a relative motion between the stator and the slider, which is pressed onto the stator. Cylindrical projections on the slider's contact surface increase the contact pressure to remove air between stator and slider. The stator is made from $LiNbO_3$. Hence, SAW can easily be generated by Inter-Digital Transducers (IDT). However, designers are restricted to a relatively expensive brittle single crystal with this setup. In contrast, an SAW motor with non-piezoelectric stator material allows for a wide range of stator materials. Previously, we built an SAW motor with a $3\,\mathrm{mm}$ thick stator made from steel type 1.4016 and presented

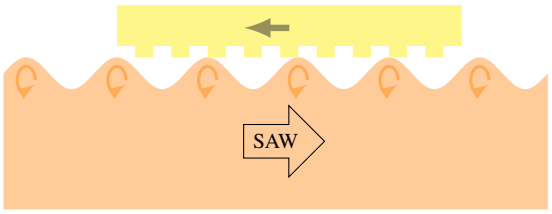

Fig. 1. Functional principle of a SAW motor: SAW travels on stator (orange) and causes a relative motion of the slider (yellow)

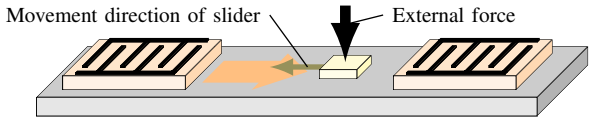

Fig. 2. Basic construction of SAW motor with non-piezoelectric stator material: Piezoelectric unit (orange block) generates SAW (orange arrow) on non-piezoelectric substrate (grey); Pressed slider (yellow) moves towards active piezoelectric unit

exemplary measurements of the motor characteristics in [7]. For SAW generation, normal polarized piezoelectric units with a thickness of $200\,\mu\mathrm{m}$ are adhered onto the roughened non-piezoelectric stator by epoxy resin as illustrated in Fig. 2. These units are made from the material *Sonox*® *P53* and are excited by IDTs with 30 finger pairs and a doubled finger spacing of $\lambda_f = 800\,\mu\mathrm{m}$. The silicon slider has 16 560 projections with a diameter of $22.5\,\mu\mathrm{m}$ and a similar setup as the slider, described in [6]. The motor achieved a blocking force of $0.19\,\mathrm{N}$ and an idling speed of $29\,\mathrm{mm\,s^{-1}}$ for a normal frequency of $3.85\,\mathrm{MHz}$ and an applied voltage amplitude of $50\,\mathrm{V}$. Furthermore, we presented Finite Element Method (FEM) models for the characterization of the piezoelectric units [7]. A modified numerical motor model that calculates motor characteristics starting from a given SAW based on [8] was used for motor characterization.

Despite our aforementioned findings in [7], practical implementations of these motors are still missing. Hence, the contribution of this paper is to present verified guidelines for designing such an SAW motor with non-piezoelectric stator material. Section II explains necessary FEM models and an improved numerical motor model in detail. Based on this, Section III presents our derived guidelines, which

This is the authors' version of this work. Please cite as R. Günther, R. Richter, J. Lienig "Design of Surface Acoustic Wave Motors With Non-piezoelectric Stator Material," Proc. Sixth Int. Conf. on Advances in Sensors, Actuators, Metering and Sensing, pp. 45-50, Nice, France, July 2021.

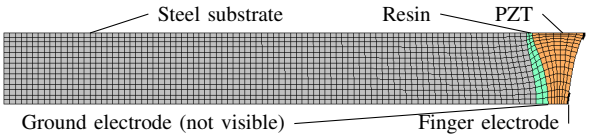

Fig. 3. FEM model for modal analysis of SAW generating unit on steel substrate

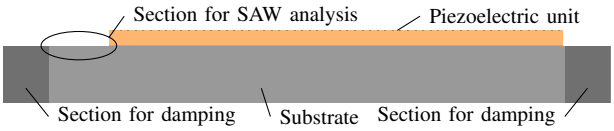

Fig. 4. Basic structure of transient FEM model

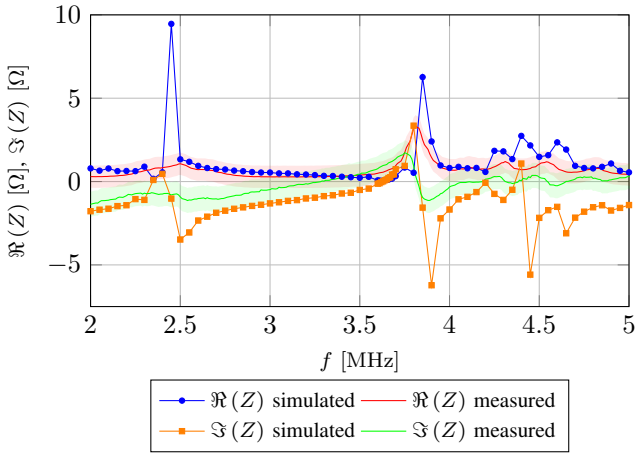

Fig. 5. Frequency dependent simulated and measured impedances for stator made from non-piezoelectric material; Measurement uncertainty is displayed transparently [7]

allow the design and implementation of advanced motors and thus support future applications of this new actuator principle. Finally, Section IV summarizes the importance of the presented guidelines for future works.

II. Numerical Models

A. Finite element models

Our two-dimensional FEM models consider the elasticity matrix, piezoelectric constants, permittivity and density for the piezoelectric material. The remaining materials are defined by *Young's* modulus, *Poisson's* ratio and density.

1) Modal analysis: According to Fig. 3, the first model takes into account only a section with the length of one finger spacing $\lambda_f/2$. With the constraint of preventing translation in the direction of propagation at boundary, it describes a stator and piezoelectric unit with infinite length. It can be used for modal analyses to determine the approximate working frequency f, which depends on the thickness of piezoelectric unit. The element size is $\lambda_f/18 \times \lambda_f/18$. It is important to set the piezoelectric constants to zero, because at resonance the power supply provides the displacement current for the actuator.

2) Transient analysis: A second model describes the whole piezoelectric unit, followed by a section with exposed stator material and a section with strong damping at each side as shown in Fig. 4. Thus, we can describe a realistic excitation of the piezoelectric unit and study the traveling SAW. The damped sections avoid a standing SAW due to reflections at the edges. The element size is $\lambda_f/25 \times \lambda_f/25$ at the top surface and increases to $\lambda_f/25 \times \lambda_f/2.5$ at the bottom due to a smaller calculation time. The time step size is $1/40f$.

For excitation of the piezoelectric unit, a sinusoidal voltage with the amplitude $\hat{U}$ is applied at the IDT. A displacement due to the SAW can be observed. Furthermore, we can read out the amplitude $\hat{q}$ and phase ϕ_q of the electric charge q of the piezoelectric unit. This allows us to determine the electric impedance Z:

$$Z = \frac{\hat{U}}{2\pi f \hat{q}} \mathrm{e}^{-\mathrm{i}\left(\phi_q + \frac{\pi}{2}\right)}. \tag{1}$$

If the dielectric loss $\tan\delta$ is significant, it can be considered as follows:

$$Z_{\tan\,\delta} = \Re(Z) + \tan\delta\,|\Im(Z)| + \mathrm{i}\Im(Z). \tag{2}$$

The impedance curves of the stator, presented in [7], are shown in Fig. 5. The higher amounts of impedance at resonances are noteworthy. The distinctive resonance of the simulation model is based on the absence of tolerances. The resonance frequencies are slightly shifted due to material and manufacturing deviations. The simulated normal displacement of stator's surface is $5487\,\mathrm{pm\,V^{-1}}$ at a frequency of $3.63\,\mathrm{MHz}$. This displacement is 17 times higher than the according measurement, with $(314 \pm 76)\,\mathrm{pm\,V^{-1}}$ at a frequency of $3.80\,\mathrm{MHz}$ [7]. The large difference can be explained by the smaller real part of the impedance for resonance with $\Re(Z\,(3.63\,\mathrm{MHz})) = 45.0\,\mathrm{m\Omega}$, according to Fig. 5, compared to the measured resistance of $\Re(Z\,(3.80\,\mathrm{MHz})) = 3.17\,\Omega$. Consequently, there is a smaller difference between simulated and measured SAW power. While the simulated efficiency is $30\,\%$, the measurement shows an efficiency of $(16.9 \pm 9.7)\,\%$. For calculation of efficiencies, the SAW power can be derived from displacement equations of *Rayleigh* waves [9] and by the definition of electric power:

$$P_{el} = 0.5\Re(S_{el}) = 0.5\Re\left(\frac{u^2}{Z}\right) = 0.5\Re\left(\frac{\hat{U}^2}{2Z}\right). \tag{3}$$

Here, S_{el} and u are the complex electric power and voltage, respectively. The factor 0.5 results from the fact that two SAW were generated by the piezoelectric unit.

B. Numerical motor model

Our numerical motor model is based on an existing model presented in [8], which considers the contact between one projection and the stator. This contact is described by normal and tangential stiffnesses of the slider $K_{sl\,n}$ and $K_{sl\,t}$ and the stator $K_{st\,n}$ and $K_{st\,t}$, respectively, as shown in Fig. 6. The stator's normal and tangential displacements $d_{st\,n}(t)$ and

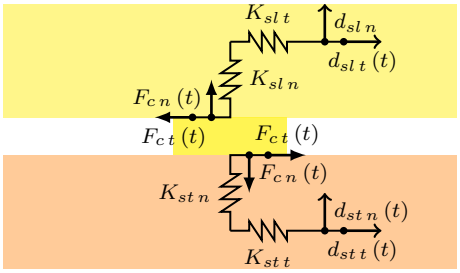

Fig. 6. Contact mechanics at one projection, used for the numeric motor model

$d_{st\,t}\,(t)$, respectively, are given by the SAW. Furthermore, we can define a normal offset $d_{sl\,n}$ of the slider. We can observe a phase with contact and a phase without contact within one period. When there is contact, the tangential force $F_{c\,t}\,(t)$ cannot exceed the normal force $F_{c\,n}\,(t)$ multiplied with the friction coefficient. If the tangential force is smaller, we notice sticking. If it is bigger, the force is limited and we notice slipping. The average force over one period equals the feed force of the considered projection. Defining a time dependent tangential slider displacement $d_{sl\,t}\,(t)$, we can consider different points of the motor characteristic. Considering all projections in a line orthogonal to the direction of SAW propagation, we can multiply the feed force by the number of projections in a line. Furthermore, it is possible to determine the friction power of the projection line and substract it from the initial SAW power. The equations for *Rayleigh* waves [9] allow for determining the new SAW amplitude at the next projection line. This procedure is repeated until all projections of the slider have been considered. Thus, the motor model is able to calculate velocity-force-diagrams. The input parameters are the density and elastic behavior of the contact materials, the normal force, the friction coefficient, the geometry and number of projections, and the frequency and amplitude of SAW. The model shows a positive influence of a high number of projections on the motor characteristic while maintaining the overall contact surface [14]. Furthermore, high friction coefficients and *Young's* moduli improve the motor's behavior.

This initial model uses an effective factor of 0.6. This means, in one direction only $60\,\%$ of the projections will contact the stator. Considering both directions, only $36\,\%$ of all projections will be used. A logical explanation for that factor would be the roughness and flatness of stator and slider. However, in this case the factor should be dependent on the pressing force. As roughness and flatness are important parameters for motors with a polycrystalline stator, the motor model was expanded by a realistic definition of the effective factor in [7]. If the slider is placed over the stator without contacting it, we could determine a distance for each projection towards the stator. Shifting the slider towards the stator, we observe a contact force when the first projection is contacted. Progressively more projections get in contact and their contact forces will be added up. For a large amount of projections and normal distributed projection distances, the total contact force can be described as follows:

$$F_N = n_{pr} K_{ov\,n} \int_{-\infty}^{d_{sl\,n}} N\left(d_n, R_a\right)\, dd_n \tag{4}$$

where n_{pr} is the number of all slider's projections and $K_{ov\,n}$ is the combined normal stiffness of slider and stator for one projection. The value $N\left(d_n, R_a\right)$ is the cumulative distribution function of the distances, d_n the current displacement of the slider, R_a the average roughness value and $d_{sl\,n}$ the slider displacement for the sought contact force. Therefore, the motor model integrates iteratively until the sought force is reached. Then the roughness dependent effective factor is given by:

$$\eta_{ro} = \sqrt{N\left(d_{sl\,n}, R_a\right)}. \tag{5}$$

Often the flatness can be described by a spherical shape, where the corresponding distances are not normally distributed. In this case, we can determine the amount of contacted projections by *Hertzian* contact theory. For a given sphere radius R_{sp}, the contact radius R_c can be calculated as follows [10]:

$$R_c = \sqrt[3]{\frac{3 F_N R_{sp}}{4 D^\star}}, \tag{6}$$
$$\text{with } \frac{1}{D^\star} = \frac{1-\nu_{st}^2}{D_{st}} + \frac{1-\nu_{sl}^2}{D_{sl}}.$$

Here, D_{sl} and D_{st} are the Young's moduli of the slider and the stator, respectively, and ν_{sl} and ν_{st} are the Poisson's ratios of the slider and the stator, respectively. Using this contact radius, the flatness effective factor can be determined as follows:

$$\eta_{fl} = \sqrt{\frac{\pi R_c^2}{b_{sl}^2}} = \frac{\sqrt{\pi}}{b_{sl}} \sqrt[3]{\frac{3 F_N R_{sp}}{4 D^\star}} \tag{7}$$

where b_{sl} is the edge length of the quadratic slider. Finally, the overall effective factor is given by:

$$\eta = \eta_{ro} \cdot \eta_{fl}. \tag{8}$$

Fig. 7 shows calculated motor characteristics for several spherical elevations and roughnesses for the mentioned SAW motor with non-piezoelectric stator material, a normal SAW amplitude of $3\,\mathrm{nm}$ at the surface, and an overall contact force of $4\,\mathrm{N}$. We can see that the flatness of $33\,\mathrm{nm}$ for the slider length of $4\,\mathrm{mm}$, which is feasible by lapping, is uncritical. However, we observe that the attainable roughness of $4.4\,\mathrm{nm}$ on the used steel downgrades the motor characteristic.

In addition, we expand the existing motor model by considering dynamic losses. Discrete *Fourier* transform allows to calculate the power of a bandlimited signal [11]. Thus, the periodic contact force curves can be decompositioned into

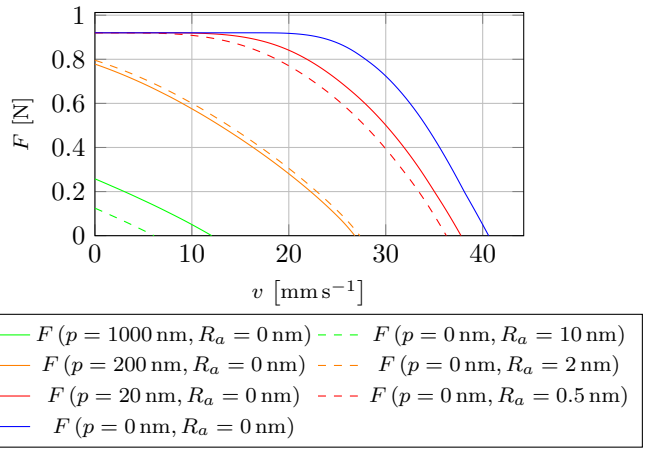

Fig. 7. Motor characteristics by motor model depending on varying spherical elevations p and average roughness values R_a; Motor as described in [7] with a normal SAW amplitude of 3 nm at the surface and an overall contact force of 4 N

harmonic forces F_f by discrete *Fourier* transform of O-th order [12]:

$$\begin{aligned} F_f =& g_0 + \sum_{j=1}^{O} \left(g_j \cos 2\pi f j t + o_j \sin 2\pi f j t\right), \\ \text{with } g_j =& \frac{2 \sin \frac{\pi j}{n_p}}{\pi j} \sum_{m=0}^{n_p-1} \left(F_m \cos \frac{2\pi j m}{n_p}\right) \\ \text{and } o_j =& \frac{2 \sin \frac{\pi j}{n_p}}{\pi j} \sum_{m=0}^{n_p-1} \left(F_m \sin \frac{2\pi j m}{n_p}\right) \end{aligned} \tag{9}$$

where g_j and o_j are the j-th *Fourier* coefficients for even and odd functions, respectively. The value F_m is the force at the discrete point m and n_p is the number of discrete points for one period. For normal and tangential harmonic excitations of circular regions on an elastic half space the mechanical impedances $Z_{M\,n}$ and $Z_{M\,t}$, respectively, can be described as follows [13]:

$$\begin{aligned} Z_{M\,n} &= \frac{4\mu R_p}{2\pi f\,(1-\nu)} \left(B_{n\,2\,1}\xi + B_{n\,2\,2}\xi^3 + \mathrm{i}\left(B_{t\,1\,1}\xi^2 - 1\right)\right), \\ Z_{M\,t} &= \frac{4\mu R_p}{2\pi f\left(1-\frac{\nu}{2}\right)} \left(B_{t\,2\,1} - B_{t\,2\,2}\xi^3 + \mathrm{i}\left(B_{t\,1\,1}\xi^2 - 1\right)\right) \\ &\text{with } \xi = \frac{2\pi f R_p}{c_T} < 0.7. \end{aligned} \tag{10}$$

Here, μ is the second *Lamé* constant, R_p is the projection radius and $B_{n\,j\,m}$ and $B_{t\,j\,m}$ are numerically determined coefficients for normal and tangential direction, respectively. The value c_T describes the transversal wave velocity. For a mechanical impedance, the dynamic power loss can be determined as follows:

$$P_\mathrm{d} = \Re\left(\frac{\hat{F_j}^2}{2Z_\mathrm{M}}\right). \tag{11}$$

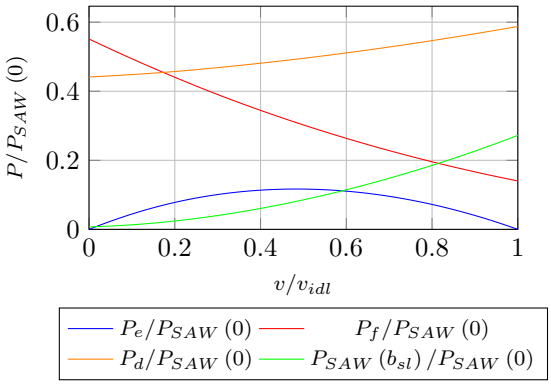

Fig. 8. Calculated effective power P_e, friction losses P_f, dynamic losses P_d and remaining SAW power P_{SAW} behind the slider for a SAW motor as described in [14]; Total contact force $F_N = 80$ N; Assumed roughness $R_a = 1$ nm due to used thin-film technology

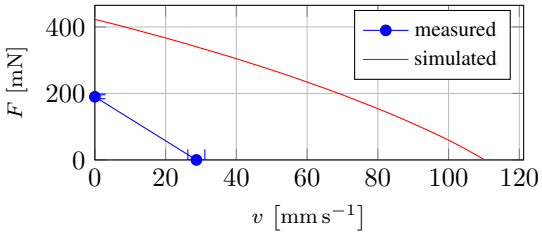

Fig. 9. Measured and simulated characteristic of SAW motor with non-piezoelectric stator material

The dynamic loss of one projection is the sum of normal and tangential dynamic power losses of all j terms, corresponding to the *Fourier* polynominal. Fig. 8 shows the power components, calculated with this expanded motor model belonging to the SAW motor presented in [14]. It is obvious that dynamic losses cannot be neglected for high contact forces.

The comparison of measured motor parameters with calculated motor characteristics in Fig. 9 reveals a clear deviation between numerical model and manufactured motor. Analyzing the measured normal displacements on the manufactured stator, according to Fig. 10, suggests a moderate SAW quality. A high standing wave ratio close to the piezoelectric unit indicates parasitic bulk waves, emitted from the piezoelectric unit and reflected at the ground. Noticeable amplitude variation suggests inhomogenities of the stator. Roughness can be eliminated as an explanatory factor. However, the steel plate was heated and cooled down slowly to release material tensions and allow a high quality of flatness by lapping. This affects grain sizes in the scale of SAW wavelength and can cause the observed SAW quality issues [15]. Bulk waves can be reduced by a higher number of finger electrodes. Different manufacturing technologies or even other steel grades will decrease the grain size. We assume that both improvements will significantly reduce the gap between measurements and simulation.

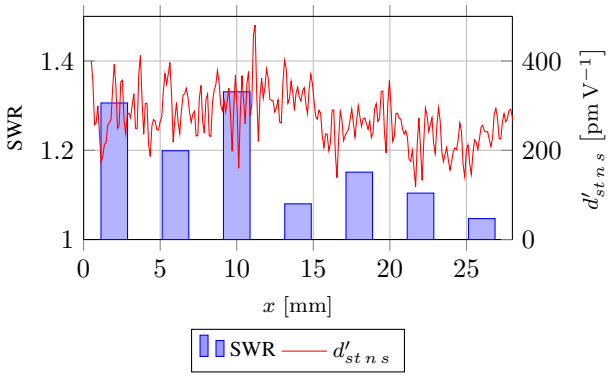

Fig. 10. Measured standing wave ratio (SWR) and relative amplitude $d'_{st,\,n\,s}$ of normal displacement of substrate surface along SAW traveling direction for SAW motor with non-piezoelectric stator material; SWR was sectionally determined by method of least squares

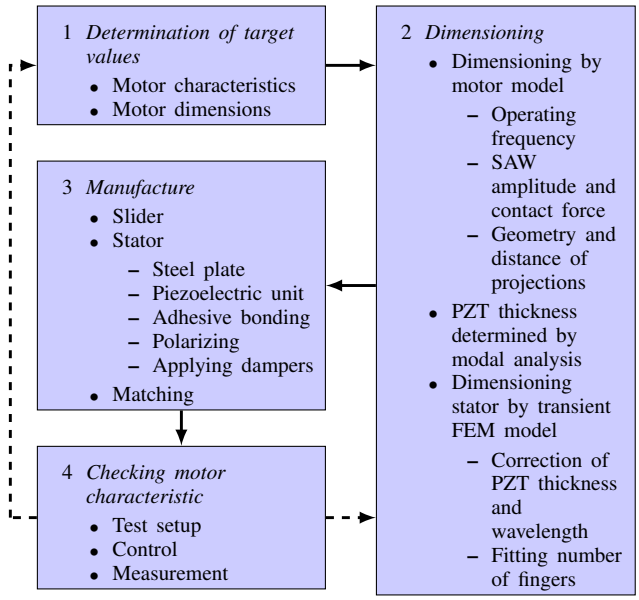

Fig. 11. Proposed procedure for designing SAW motors with steel stator

III. Guidelines for Designing

This section presents the working steps to design and manufacture an SAW motor with non-piezoelectric stator material based on specified characteristics. These guidelines are the result of experiences we gathered by developing, manufacturing and testing the SAW motor. They are limited to motors with a PZT unit adhered on metallic substrate and a slider made from silicon. Refeeding of remaining SAW power is not considered. Our presented procedure is also visualized in Fig. 11.

1 *Determination of target values*

- Motor characteristics: Define blocking force and idling speed.
- Motor dimensions: The width of the motor is proportional to motor power by constant SAW amplitude. The length of the motor results from travel range and the dimensions of piezoelectric units and dampers.

2 *Dimensioning*

- Dimensioning by motor model:
  - Operating frequency: Higher operating frequencies result in higher idling speeds and lower blocking forces.
  - SAW amplitude and contact force: Here an optimization process is needed. The main target is to reach specified motor characteristic. The secondary target is to minimize the SAW amplitude for a higher efficiency.
  - Geometry and distance of projections: Projection diameters of about $20\,\mu\mathrm{m}$ and projection spacings of about $40\,\mu\mathrm{m}$ have been found as ideal structuring geometry in [16]. In addition, the efficiency of extraordinary motor characteristics can be optimized by varying that geometry.
- PZT thickness determined by modal analysis: Specify finger spacing by operating frequency and SAW speed. Vary thickness of PZT to reach targeted frequency for the first symmetric *Sezawa* mode.
- Dimensioning stator by transient FEM model:
  - Correction of PZT thickness and finger spacing: Vary parameters within an optimization to maximize the SAW displacement per voltage and the efficiency.
  - Fitting number of fingers: Vary this parameter to reach the relative SAW displacement, while respecting dielectric strength, tensile strengths and depolarization. As we observed a much higher relative SAW amplitude in simulation related to measurements, we recommend a safety of 30 for depolarization.

3 *Manufacture*

- Slider: Thin-layer technology is to be used without any special features.
- Stator:
  - Metal plate: Thickness must be more than triple wavelength. Lap and polish the stress-relieved plate. Roughen the bonding surface.
  - Piezoelectric unit: Saw out the PZT plate. Sputter a ground electrode on one side. Apply IDT by thick film technology on the other side. Both electrodes are made from gold.
  - Adhesive bonding: Ensure an electric contact between ground electrode and metal plate for later polarization. Furthermore, a mechanical wide-area contact with thin adhesive layer thickness is needed for a good transmission.
  - Polarizing: For normal polarization with $2\,\mathrm{MV\,m^{-1}}$, conductive silver lacquer must be applied on the top surface and removed afterwards. Correct application and removing can be checked by resistance measurements.

  - Applying dampers: Apply viscoelastic material behind the piezoelectric units over a distance of ten wavelengths.
- Matching: Build up an impedance matching considering the measured stator impedance at operation frequency.

4 *Checking motor characteristic*

- Test setup: Connect stator with impedance matching, amplifier and waveform generator. Stator voltage can be checked directly by oscilloscope. Clean contact surfaces. Attach slider and magnets with iron counterplate carefully onto the stator.
- Control: Depending on input power drive the motor only in burst mode with sinusoidal excitation.
- Measurement: Measure idling speed by laser triangulation sensor and blocking force by force measuring device with force transducer crossing the travel path.

IV. Conclusion

We have presented detailed guidelines for designing a novel type of SAW motor with non-piezoelectric stator material. Required numeric models are extensively described and discussed as well. With this, we enable manufacturing and further investigations into this motor type to improve its characteristics. We are optimistic that these improvements lead to compact linear motors with a high positioning accuracy, high power density and, moreover, an inexpensive manufacturing. The presented models and resulting verified guidelines should contribute to a market launch of SAW motors that will support the growing demand for compact linear actuators.

Acknowledgment

The authors would like to thank Hagen Schmidt and Robert Weser of the Leibnitz Institute for Solid State and Materials Research in Dresden for the recurring friendly support with measurement equipment and professional advices. We also thank Sylvia Gebhardt and Susanne Tilke of the Fraunhofer Institute for Ceramic Technologies and Systems IKTS for the manufacture and mounting of piezoelectric units.

References

[1] F. Zhang, W. Chen J. Lin, and Z. Wang, “Bidirectional linear ultrasonic motor using longitudinal vibrating transducers” IEEE Transactions on Ultrasonics, Ferroelectrics, and Frequency Control, IEEE, vol. 52.1, pp. 134–138, 2005. DOI: 10.1109/TUFFC.2005.1397358.

[2] K. Spanner, O. Vyshnevskyy, and W. Wischnewskiy, “New linear ultrasonic micromotor for precision mechatronic systems” Proceedings of the 10th International Conference on New Actuators (Actuator 2006), pp. 439–443, 2006.

[3] Y. Shi and C. Zhao, “A new standing-wave-type linear ultrasonic motor based on in-plane modes” Ultrasonics, Elsevier, vol. 51.4, pp. 397–404, 2011.

[4] Z. Wan and H. Hu, “Modeling and experimental analysis of the linear ultrasonic motor with in-plane bending and longitudinal mode”, Ultrasonics, Elsevier, vol. 54.3, pp. 921–928, 2014. DOI: 10.1016/j.ultras.2013.11.004.

[5] M. Guo, S. Pan, J. Hu, C. Zhao, and S. Dong, “A small linear ultrasonic motor utilizing longitudinal and bending modes of a piezoelectric tube”, IEEE Transactions on Ultrasonics, Ferroelectrics, and Frequency Control, IEEE, vol. 61.4, pp. 705–709, 2014. DOI: 10.1109/TUFFC.2014.2958.

[6] T. Shigematsu, M. K. Kurosawa, and K. Asai, “Nanometer stepping drives of surface acoustic wave motor”, IEEE Transactions on Ultrasonics, Ferroelectrics, and Frequency Control, IEEE, vol. 50.4, pp. 376–385, 2003. DOI: 10.1109/TUFFC.2003.1197960.

[7] R. Günther, R. Richter, and J. Lienig, “Contributions to the development of an axisymmetric SAW motor with a stator made from non-piezoelectric material”, Sensors and Actuators A: Physical, Elsevier, vol. 295, pp. 274–287, 2019. DOI: 10.1016/j.sna.2019.04.024.

[8] T. Shigematsu and M. K. Kurosawa, “Friction drive modeling of SAW motor using classical theory of contact mechanics”, Proc. of 10th Conf. on New Actuators, pp. 444–448, 2006.

[9] I. A. Viktorov, “Rayleigh and Lamb Waves: Physical Theory and Applications: Translated from Russian”, Plenum press, 1967.

[10] K. L. Johnson, “Normal contact of elastic solids – hertz theory”, Contact Mechanics, Cambridge University Press, Ch. 4, pp. 84–106, 1985.

[11] J. L. Brown, “Sampling bandlimited periodic signals–an application of the DFT”, IEEE Transactions on Education, IEEE, vol. 23.4, pp. 205–206, 1980. DOI: 10.1109/TE.1980.4321415.

[12] G. Merziger, G. Mühlbach, D. Wille, and T. Wirth, “Folgen, Reihen [Sequences, Series]”, Formeln + Hilfen zur höheren Mathematik [Formulas + Helps for higher mathematics], Binomi, Edition 3, p. 76, 1999.

[13] G. M. L. Gladwell, “The calculation of mechanical impedances relating to an indenter vibrating on the surface of a semi-infinite elastic body”, Journal of Sound and Vibration, vol. 8.2, pp. 215–228, 1968. DOI: 10.1016/0022-460X(68)90228-9.

[14] M. K. Kurosawa and T. Shigematsu, “Friction drive simulation of a SAW motor with slider surface texture variation”, Advances in Science and Technology, Trans Tech Publ., vol. 54, pp. 366–371, 2008. DOI: 10.4028/www.scientific.net/AST.54.366.

[15] A. Fattah-Alhosseini and S. Vafaeian, “Comparison of electrochemical behavior between coarse-grained and fine-grained AISI 430 ferritic stainless steel by Mott-Schottky analysis and EIS measurements”, Journal of Alloys and Compounds 639, pp. 301–307, 2015. DOI: 10.1016/j.jallcom.2015.03.142.

[16] M. K. Kurosawa, H. Itoh, K. Asai, M. Takasaki, and T. Higuchi, “Optimization of slider contact face geometry for surface acoustic wave motor”, The 14th IEEE International Conference on MEMS, pp. 252–255, 2001. DOI: 10.1109/MEMSYS.2001.906526.

This is the authors' version of this work. Please cite as R. Günther, R. Richter, J. Lienig "Design of Surface Acoustic Wave Motors With Non-piezoelectric Stator Material," Proc. Sixth Int. Conf. on Advances in Sensors, Actuators, Metering and Sensing, pp. 45-50, Nice, France, July 2021.